Turkish Journal of Electrical Engineering & Computer Sciences

http://journals.tubitak.gov.tr/elektrik/

Research Article

Turk J Elec Eng & Comp Sci
(2016) 24: 2556 – 2574

doi:10.3906/elk-1403-57

Fuzzy logic based voltage control scheme for improvement in dynamic response of the class D inverter based high frequency induction heating system

Booma NAGARAJAN*, **Rama Reddy SATHI**, **Pradeep VISHNURAM**
Department of Electrical and Electronics Engineering, Jerusalem College of Engineering,
Centre for Collaborative Research with Anna University, Chennai, Tamil Nadu, India

Received: 08.03.2014 • **Accepted/Published Online:** 28.09.2014 • **Final Version:** 15.04.2016

Abstract: In high frequency induction heating systems, the effective load parameters change during the different operating conditions. It is necessary to maintain constant input voltage to the induction heating load to improve the quality of the heating. The resonant based high frequency converter is generally used for these applications for the reduction of switching losses. The resonant condition is also affected during the variation in load parameters. The controller should provide a good voltage regulation with less response time and less overshoot during the loading conditions. In this paper, a load adaptive fuzzy logic control scheme is proposed to perform the voltage control of the high frequency inverter under variable load conditions. A frequency tracking control system is also employed for the inverter system using the phase lock loop. The phase lock loop ensures the resonant frequency operation of the inverter during the change in load parameters. The state space model of the system is discussed to study the inverter during different operating conditions. The fuzzy logic controller based closed loop control scheme is developed using the MATLAB simulation tool. The responses of the conventional and fuzzy logic controllers are studied for load voltage regulation and the effectiveness of the control schemes is verified. The dynamic behavior of the system is studied under no load and loaded conditions with the two controllers. The fuzzy based closed loop control scheme improves the dynamic response of the system compared to the conventional controller. The response of the induction heating system is validated with a hardware prototype. The results are presented in order to confirm the proposed control strategy.

Key words: Fuzzy logic control, proportional-integral-derivative controller, induction heating, state space modeling

1. Introduction

Induction heating (IH) has become the popular choice of technology for industrial and domestic applications due to its advantages such as safety, efficiency, and cleanliness when compared with the other classical heating methods. The IH load has to be controlled accurately and smoothly in order to supply the desired temperature level to the workpiece [1,2]. The temperature of the workpiece in the IH system is regulated by means of the electric power transferred to it.

The resonant inverter is mainly used in the design of the IH power supply system to achieve the desired performance and efficiency. Several resonant inverter configurations have been used in IH applications: single-switch, half bridge, and full bridge inverter topologies [3–7]. Among them, the class D series resonant inverter shown in Figure 1 is the widely used topology due to its good balance between cost and performance [8]. The resonant inverter is normally operated above the resonant frequency to achieve the zero voltage switching

*Correspondence: booma_ nagarajan@yahoo.com

condition (ZVS) in the switches of the inverter [9,10]. In this way, the efficiency of the power supply system is increased. The operation of the class D series resonant inverter during the steady state condition has been analyzed in several studies [4,11–14]. There are still some challenges regarding the dynamic behavior of the system with highly variable operating conditions of the IH load.

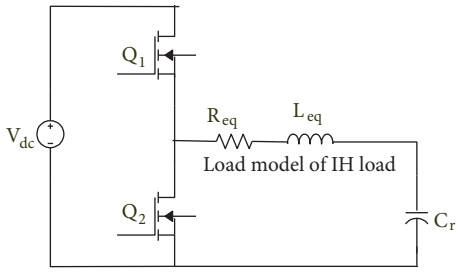

Figure 1. Schematic of class D inverter for IH applications.

The IH system consists of an induction coil in which the workpiece has to be kept inside. During this process, the effective voltage applied to the work coil becomes decreased due to the variation in the effective impedance of the load and the coil. The effective impedance also varies under the steady state operating conditions due to temperature, frequency, and alignment between coil-load assembly [15,16]. Maintaining the load voltage at the rated value without disturbing the resonant operation of the inverter plays an important role in the IH system during its initial loading and change in load parameter conditions [16–18]. The output voltage of the class D inverter can be maintained constant by employing a closed loop control. The closed loop controller can be used to vary the DC input voltage supplied to the IH load. For the output voltage control of the inverter, two control loops are employed. One loop adjusts the inverter switching frequency (f_s) and the other loop adjusts the amplitude of the DC input voltage (V_{dc}). To adjust the f_s, a frequency trailing system, the phase locked loop (PLL), is used. Conventionally the traditional proportional-integral-derivative (PID) controller is used to control the DC link voltage. The PID controller performs the voltage control with less accuracy and large response time. It also fails to regulate the voltage when the changes in the load parameters are nonlinear.

The literature does not deal with improvement of the dynamic response of a high frequency IH system using the fuzzy logic controller (FLC). This study proposes a FLC based control scheme to improve the dynamic performance of the inverter under the no load and load condition of the IH system. This paper discusses the closed loop control of DC link voltage using conventional and the proposed controllers under start up and variable load conditions. The performance parameters of the closed loop response with the PID controller and FLC are obtained for comparison. The proposed control system provides an improvement in dynamic response of the system in order to obtain improved performance of the IH load power supply system. Small signal modeling of the resonant power inverter is also done to analyze the dynamic response of the system. The subsections detail the main blocks of the frequency trailing system using PLL and the closed loop voltage control of the IH power supply system.

2. Description of the class-D resonant inverter based IH power supply system

The circuit configuration of the class D resonant inverter based IH power supply system with the proposed control circuit is shown in Figure 2(a). It is basically an AC-AC conversion circuit for conversion of commercial frequency AC into high frequency AC (HFAC). The converter has a controlled rectifier to convert the 50 Hz

single phase AC input voltage (V_{ac}) into DC supply. In order to filter the ripple content, a smoothing capacitor (C_B) is used. As IH load requires HFAC supply, the pure DC is then converted into HFAC by using the class-D series resonant inverter. The high frequency AC current (i_o) is applied to the IH coil, so that the workpiece gets heated up. R_{eq} and L_{eq} are the equivalent resistance and inductance parameters of the IH load and the induction coil. The resistance and inductance of the coil and the load are considered separately to study the change in voltage during the loading condition. The induction coil is modeled by its equivalent resistance (R_C) and equivalent inductance (L_C). The resistance and the inductance of the workpiece are considered as R_W and L_W.

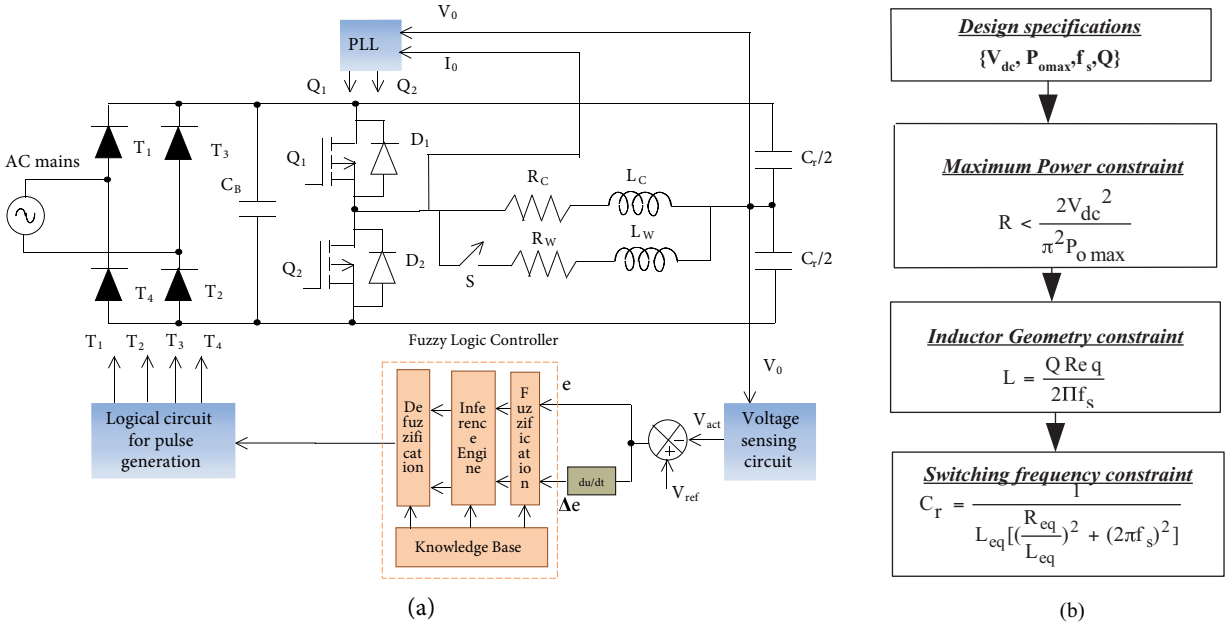

Figure 2. (a) IH power supply system with FLC based control scheme, (b) Design flow chart.

Series resonant condition is achieved using a resonant capacitor (C_r) considered equally on both sides of the inverter. The switches Q_1 and Q_2 are MOSFET switches with a small value of snubber capacitance (C_S). These switches are alternatively turned on and off with the high frequency pulses generated using the PLL. The PLL based control circuit is used to maintain the resonant operating condition of the class D inverter even with the change in the load parameters. The gate pulses for the rectifier switches are generated by the FLC to regulate the voltage applied to the IH load.

The design flow chart for the class D half bridge high frequency inverter is shown in Figure 2(b). For the maximum power, 500 W, of the designed IH load, the maximum value of IH load resistor (R_{eq}) calculated at the resonant condition is 5 Ω. The quality factor of the induction heating load (Q) depends on the external diameter, internal diameter, and number of turns of the designed inductor. For the selected IH load with a Q of 1.32, the value of the obtained series inductance (L_{eq}) is 39.7 mu H. The maximum output power is achieved at the resonant frequency. To minimize the switching losses, the switching frequency is selected above the resonant frequency. For the value of 22 kHz frequency, the calculated value of the resonant capacitor is 1.59 μF. Further the design parameters and specifications for the proposed power supply circuit are shown in Table 1.

Table 1. Design specifications.

Quantity	Symbol	Values
Initial switching frequency	f_s	22 kHz
Initial resonant frequency	f_r	20 kHz
IH load inductance	L_{eq}	0.0397e-3H
IH load resistance	R_{eq}	5 Ohms
Resonant capacitor	C_r	1.59 e-6 F
DC link capacitor	C_{dc}	5 mu F

3. State space analysis of IH power supply system

In this section, the small-signal model of the class D series-resonant inverter fed IH load is acquired. The perturbation and linearization can be executed with the switching period, by which the small signal modeling can forecast the accuracy. Consider the load current (i_o) with the capacitor voltage (V_c) and load voltage (V_o) of the equivalent circuit of series resonant inverter shown in Figure 3 could be modeled using the following state equations:

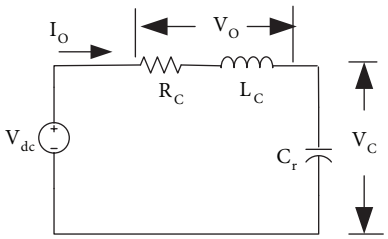

Figure 3. Equivalent circuit of series resonant inverter.

$$L_c \frac{di_o}{dt} + V_c + i_o R_c = V_{dc} \tag{1}$$

$$C_r \frac{dv_c}{dt} = \mathbf{i}_o \tag{2}$$

Under resonant condition, the output power of the converter is the power at the resistor, which is given by

$$P_o = \frac{R_c i_o^2}{2} \tag{3}$$

The harmonic approximations of the i_0 and V_c are

$$i_o(t) \approx i_v(t) \cdot \cos(\omega_s t) + i_h(t) \cdot \sin(\omega_s t), \tag{4}$$

$$v_c(t) \approx v_v(t) \cdot \cos(\omega_s t) + v_h(t) \cdot \sin(\omega_s t), \tag{5}$$

The load voltage describing function is given by

$$V_o = \frac{2}{\pi} V_{dc} \sin(2\pi D) \sin(\omega t) = v_e \sin(\omega t), \tag{6}$$

where

$$V_e = \frac{2}{\pi} V_{dc} \sin(2\pi D) \tag{7}$$

Eqs. (4)–(6) are substituted into Eqs. (1) and (2).The resulting equations are decomposed into four equations, (8)–(11), and then considered separately as sine and cosine terms using the harmonic balance procedure described below.

Sine terms:

$$\frac{dv_h}{dt} = \frac{i_h}{C_r} + \omega_s v_v, \tag{8}$$

$$\frac{di_h}{dt} = \frac{-v_h - i_h R_c + v_v}{L_c} + \omega_s i_v, \tag{9}$$

Cosine terms:

$$\frac{dv_v}{dt} = \frac{i_v}{C_r} + \omega_s v_h, \tag{10}$$

$$\frac{di_v}{dt} = \frac{-v_v - i_v R_c}{Lc} + \omega_s i_h \tag{11}$$

The linearized model is established by perturbing the large signal system given by Eqs. (8)–(11) around the operating point $[\mathrm{V}_{dc}, \mathrm{D}, \omega]$, where V_{dc}, is the input voltage, ω_s is the switching frequency, and D is the duty ratio. Eqs. (8)–(11) are solved to obtain the operating point by setting all derivatives to zero, which is given by

$$I_h = \frac{V_e \omega_s^2 C_r^2 R_c}{\psi} \tag{12}$$

$$I_v = \frac{V_e \omega_s C_r \left(1 - \omega_s^2 L_c C_r\right)}{\Psi} \tag{13}$$

$$V_h = \frac{V_e \left(1 - \omega_s^2 L_c C_r\right)}{\Psi} \tag{14}$$

$$V_v = \frac{V_e \omega_s C_r R_c}{\Psi}, \tag{15}$$

where

$$\Psi = \omega_s^4 C_r^2 L_c^2 - 2\omega_s^2 C_r L_c + \omega_s^2 C_r^2 R_c^2 + 1 \tag{16}$$

The inputs, the state variables, and the output are the perturbed variables is of the form

$$h(t) = H + \hat{h}(t), \tag{17}$$

where H is the operating point and $\hat{h}(t)$ is a small perturbation in amplitude. By using the Taylor series expansion and taking only the first order partial derivatives, the perturbed variables could be replaced in Eqs. (8)–(11) to obtain the linearized model. Eq. (9) could be written as

$$\frac{di_h}{dt} = f(v_h, v_v, i_h, i_v, D, v_e, \omega_s) \tag{18}$$

Hence, its linearized equation is

$$\frac{d\hat{v}_h}{dt} \approx \frac{\partial f}{\partial v_h}\hat{v}_h + \frac{\partial f}{\partial v_v}\hat{i}_h + \frac{\partial f}{\partial i_h}\hat{i}_v + \frac{\partial f}{\partial \omega_s}\hat{\omega}_s + \frac{\partial f}{\partial v_e}\hat{v}_e + \frac{\partial f}{\partial D}d\hat{\wedge}, \tag{19}$$

where $\frac{\partial f}{\partial x}$ is estimated at the operating points. The complete linearized model is given as

$$\frac{d\hat{v}_h}{dt} = \frac{\hat{i}_h}{C_r} + \omega_h\hat{v}_v + V_v\hat{\omega}_s \tag{20}$$

$$\frac{d\hat{i}_h}{dt} = \frac{\hat{v}_h}{L_c} - \frac{R}{L_c}\hat{i}_h + \omega_s\hat{i}_v + I_v\hat{\omega}_s + \frac{2V_e}{L_c}\cos(2\pi D)\,\hat{v}_e + \frac{2V_e}{L_c}\sin(2\pi D)\,\hat{v}_e \tag{21}$$

$$\frac{d\hat{v}_v}{dt} = \frac{\hat{i}_v}{C_r} - \omega_s\hat{v}_h - V_e\hat{\omega}_s \tag{22}$$

$$\frac{d\hat{v}_v}{dt} = \frac{\hat{v}_v}{C_r} - \frac{R_c}{L_c}\hat{i}_v - \omega_s\hat{i}_h - I_h\hat{\omega}_s \tag{23}$$

The matrix representation of the model is given as

$$\dot{x} = Ax + B_d u_1 + B_\omega u_2 \tag{24}$$

$$y = Cx, \tag{25}$$

where y is vector of the output variable and x is the state variable vector such as

$$\dot{x} = \begin{bmatrix} \hat{i}_s & \hat{i}_c & \hat{v}_s & \hat{v}_c \end{bmatrix}^T \tag{26}$$

$$y = \hat{p}_o \tag{27}$$

Thus,

$$\dot{x} = \begin{bmatrix} \frac{-R_c}{L_c} & \omega_s & \frac{-1}{L_c} & 0 \\ -\omega_s & \frac{-R_c}{L_c} & 0 & \frac{-1}{L_c} \\ \frac{1}{C_r} & 0 & 0 & \omega_s \\ 0 & \frac{1}{C_r} & -\omega_s & 0 \end{bmatrix} x + \begin{bmatrix} \frac{2}{L_c}\cos(2\pi D) \\ \frac{2}{L_c}\sin(2\pi D) \\ 0 \\ 0 \end{bmatrix} \hat{v}_{dc} + \begin{bmatrix} I_v \\ -I_h \\ V_v \\ -V_h \end{bmatrix} \hat{\omega}_s$$

$$y = [RI_h RI_v 00]\, x \tag{28}$$

The perturbed output power is given as

$$\hat{P}_o = RI_h\hat{i}_h + RI_v\hat{i}_v \tag{29}$$

The gain of the small signal duty-to-output power G_{pd}, and the frequency-to-output power, G_{pf}, are obtained by using the above equations and they are given as

$$G_{pd}(s) = \frac{\hat{p}_h}{\hat{d}} = C(sI - A)^{-1}\mathbf{B}_d \tag{30}$$

$$G_{pf}(s) = \frac{2\pi * \hat{p}_h}{\omega_{sw}} = 2\pi C(sI - A)^{-1}\mathbf{B}_{\omega} \tag{31}$$

The quality factor (Q) the coil is

$$Q = \frac{\omega_{sL}}{R} \tag{32}$$

Whenever the load parameters change, it is necessary to change the operating conditions such as duty cycle and operating frequency of the inverter. For the different operating conditions, the magnitude plots for G_{pd} and G_{pf} are displayed in Figure 4. These plots illustrate the variations in the operating condition with respect to the dynamic behavior of the system. With the change in frequency, it is necessary to maintain the closed loop stability. It is clear that the change in the induction load parameters changes the dynamic behavior of the converter. Therefore, the design of the control circuit should be such that it should be able to adapt to perturbation in the operating and load conditions. Thus the small signal modeling helps in studying the dynamic behavior of the system under various perturbations in switching frequency and various duty cycles. To change the dynamic behavior of the inverter, during perturbations in the load, the frequency trailing system is incorporated. The FLC based voltage control scheme is proposed to regulate the inverter output voltage during no load and load conditions.

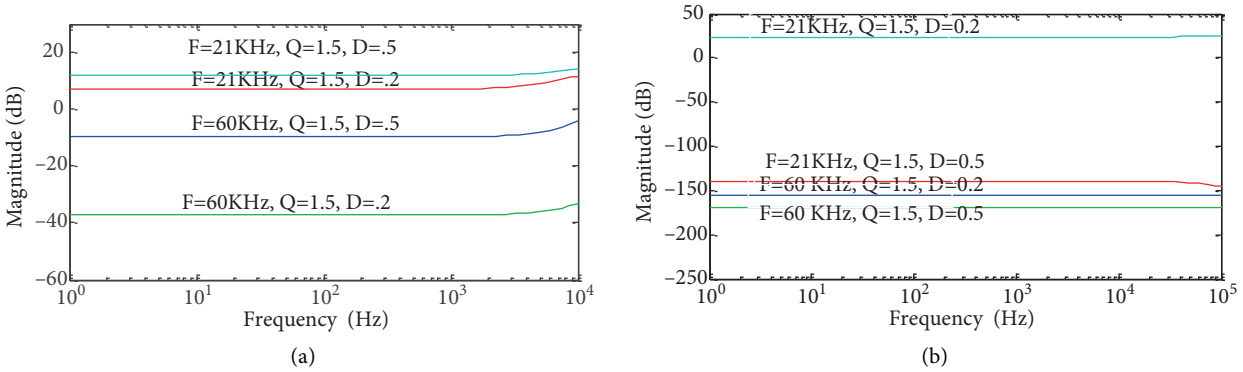

Figure 4. **(a)** Magnitude plot for different operating condition of G_{pd}, (b) Magnitude plot for different operating condition of G_{pf}.

4. Frequency trailing system for inverter

IH load is characterized by the equivalent resistance (R_c and R_w) and inductance (L_c and L_w) of its induction coil and workpiece. When the workpiece made of different material is inserted into the IH coil, its geometry, conductivity, and permeability cause change in the equivalent inductance of the load arrangement. For the reduction in switching losses it is necessary to operate the class D inverter close to the resonant frequency. When the load parameters change, there is a change in resonant operating condition. It is necessary to vary the operating frequency of the inverter due to change in parameters depending on the resonant frequency of the load circuit. Therefore, the control circuit should employ a frequency trailing system to track the resonant frequency of the newly changed load parameters.

A tuned frequency trailing system using the PLL is used to track the new frequency. It helps to maintain the zero voltage switching (ZVS) condition of the inverter switches in spite of the load parameter variation. In the inverter, the frequency tracking control method is established by changing the frequency of the pulses.

Figure 5(a) shows the block diagram of the PLL based control circuit developed for the class D inverter. The PLL circuit causes one signal to track the other signal. It keeps the output signal synchronized with the reference signal with respect to the phase and the frequency. The PLL circuit achieves the phase lock control between I_o and V_o. It maintains the switching frequency close to the resonant frequency in order to achieve the ZVS [19–21]. It consists of a phase detector (PD), a low-pass filter (LPF), and a voltage-controlled oscillator (VCO). The zero crossing instant of the output current signal was compared with the zero crossing instant of the output voltage signal in order to detect the difference in phase. The PD compares the phase angle of the two inputs $\varphi_1(t)$ and $\varphi_2(t)$ and generates an error signal $\Delta\varphi(t)$. The error signal is proportional to the phase difference between the two inputs and the gain (K_D). The output of the PD is given by

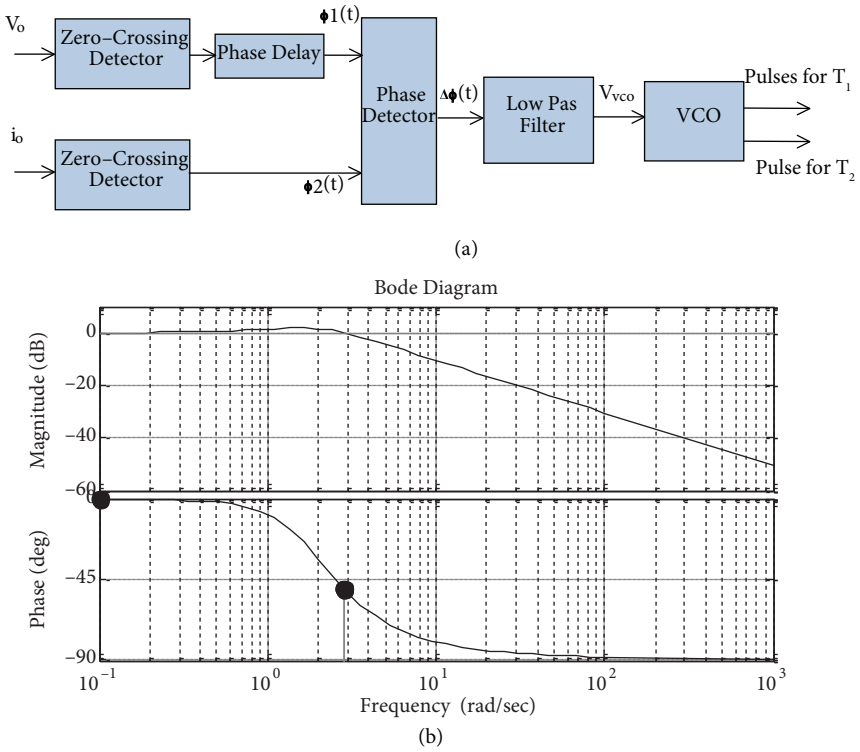

Figure 5. (a) Block diagram of PLL, (b) Bode plot of PLL

$$\Delta\varphi(t) = K_D\left[\Delta\varphi_1(t) - \Delta\varphi_2(t)\right] \tag{33}$$

The two inputs to the PD are depicted as square waves, producing an output pulse $\Delta\varphi(t)$ whenever there is a phase misalignment. The output signal from the PD is filtered by the low pass filter, which is basically a PI compensator, to get an average value of the voltage. The average voltage confirms the phase difference between load voltage and load current. The transfer function of the LPF (F(s)) is given by

$$F(s) = \frac{V_{VCO}}{\Delta\varphi(t)} = K_p + \frac{K_i}{S} \tag{34}$$

The output of the PI compensator is the average value of the error voltage. This error signal changes the output frequency of the oscillating signal produced by the voltage control oscillator (VCO) in order to maintain

the phase angle when the parameters of the IH load are varied. The VCO oscillates slightly greater than the resonant frequency, to drive the inverter in ZVS mode. VCO with a gain (K_{vco}) produces the switching pulses at the tracked frequency. The transfer function of the VCO (K_v) is given by

$$K_v = \frac{K_{VCO}}{S} \tag{35}$$

When the frequencies of the I_o and V_o are unequal, the PD gives an output signal indicating a frequency difference and when locked it indicates a phase difference. The output signal of the PD is used to shift the VCO toward lock before capture, and then holds the frequency in lock. Under the locked condition, I_o and V_o signals have the same frequency. The VCO output signal is directly fed to the switches of the inverter.

By considering the fixed resonant capacitance, the tank circuit is driven to its new resonant frequency by tracking the switching frequency of the inverter. Dynamic ZVS can be achieved in switches of the inverter, since the PLL circuit tracks the resonant frequency corresponding to equivalent load parameters. Figure 5(b) shows the Bode diagram of PLL with the gain $G_{PLL}(S)$. The gain of the PLL is given by

$$G_{PLL} = K_p * (K_p + \frac{K_i}{S}) * \frac{K_{vco}}{S} \tag{36}$$

The obtained frequency domain parameters from the frequency plot of the system ensure the stability of the PLL loop.

5. Closed loop voltage control of IH system

5.1. Design and description of the PID controller

Class-D inverter fed IH systems are used for low and medium power applications in industrial and domestic usages. The variations in the effective impedance during the initial loading, heating process, and load fluctuations disturb the resonant operation. The PLL based frequency tracking system is used to operate the inverter at resonant condition. Due to the variations in the electrical parameters, the effective voltage across the work coil is decreased. A closed loop control system is developed to regulate the output voltage of the inverter by controlling the pulse width of the gate pulses applied to the switches of the rectifier.

The schematic of the class-D resonant inverter based IH power supply system with the conventional PID controller is illustrated in Figure 6. The system is simulated using the switching models of the power electronic converters together with control environment in MATLAB software. The resistance and inductance of the work coil could be represented as R_c and L_c, respectively. Whenever the switch (S) is closed, the workpiece with resistance R_w and inductance L_w is added to the system. This changes the value of the equivalent resistance and inductance of the IH load. The changes in equivalent parameters cause the dip in the inverter output voltage. The error in voltage (e(s)) is processed by the PID controller. The control signal Q(s) at the output of the PID controller is given as

$$Q(s) = \left(K_p + \frac{K_i}{S} + S K_d \right) * [e(s)], \tag{37}$$

where K_p, K_i, and K_d are the gains of the PID controller designed at the given operating condition. Initial design of the gains K_p, K_i, and K_d is carried out using the small-signal model of the class-D resonant inverter and the Ziegler–Nichols technique [22,23]. The PID controller regulates the voltage with a large peak overshoot, settling time, and steady state error. The limitations also arise due to its linear nature whereas the variations in

the IH load parameters are nonlinear. To improve the dynamic response of the system and to solve uncertainty problems due to variations in load parameter, the fuzzy-logic control scheme is proposed.

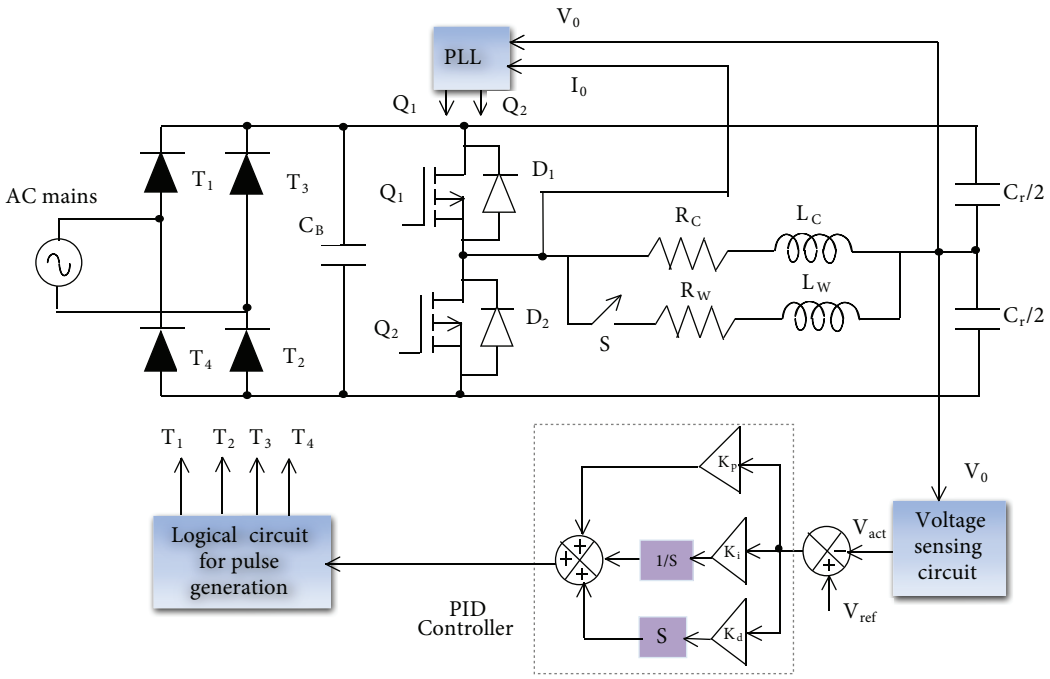

Figure 6. Closed loop control architecture for class-D resonant converter with PID controller.

5.2. Design of the FLC for the IH power supply system

In recent years, the FLC has been widely used for many industrial applications due to its heuristic nature associated with simplicity. The control of the FLC is effective for both linear and nonlinear systems. This section briefly describes the design of the FLC for voltage control in IH applications. The basic structure of a fuzzy controller used in this work is shown in Figure 7(a). Fuzzy controllers are based on four well-known stages: fuzzification, fuzzy rule base, inference engine, and defuzzification. The first stage is fuzzification, which is the process of making of a crisp quantity fuzzy, which is done by recognizing many quantities considered crisp and deterministic that are actually not deterministic at all, which carries considerable uncertainty. If the form of uncertainly happens to arise because of imprecision ambiguity or vagueness, then the variable is probably fuzzy and can be represented by a membership function. In the fuzzification process, the numerical variable is converted into a linguistic variable. The controlling inputs of the FLC are error (e) and change in error (Δe). The following seven fuzzy levels are chosen for the controlling inputs error and change in error of the fuzzy controller in the fuzzification: large negative (LN), medium negative (MN), small negative (SN), zero (Z), large positive (LP), medium positive (MP), and small positive (SP). In addition to these levels, the output variable (U) has two extra levels: very large negative (VLN) and very large positive (VLP).

Membership functions for controller inputs, i.e., e, Δe, and the controller output (U), are defined on the common normalized range of [–1, 1]. The symmetric triangles with equal base are considered as the membership functions. They have 50% overlap with the neighboring function. The input and output membership functions for the FLC are shown in Figure 7(b).

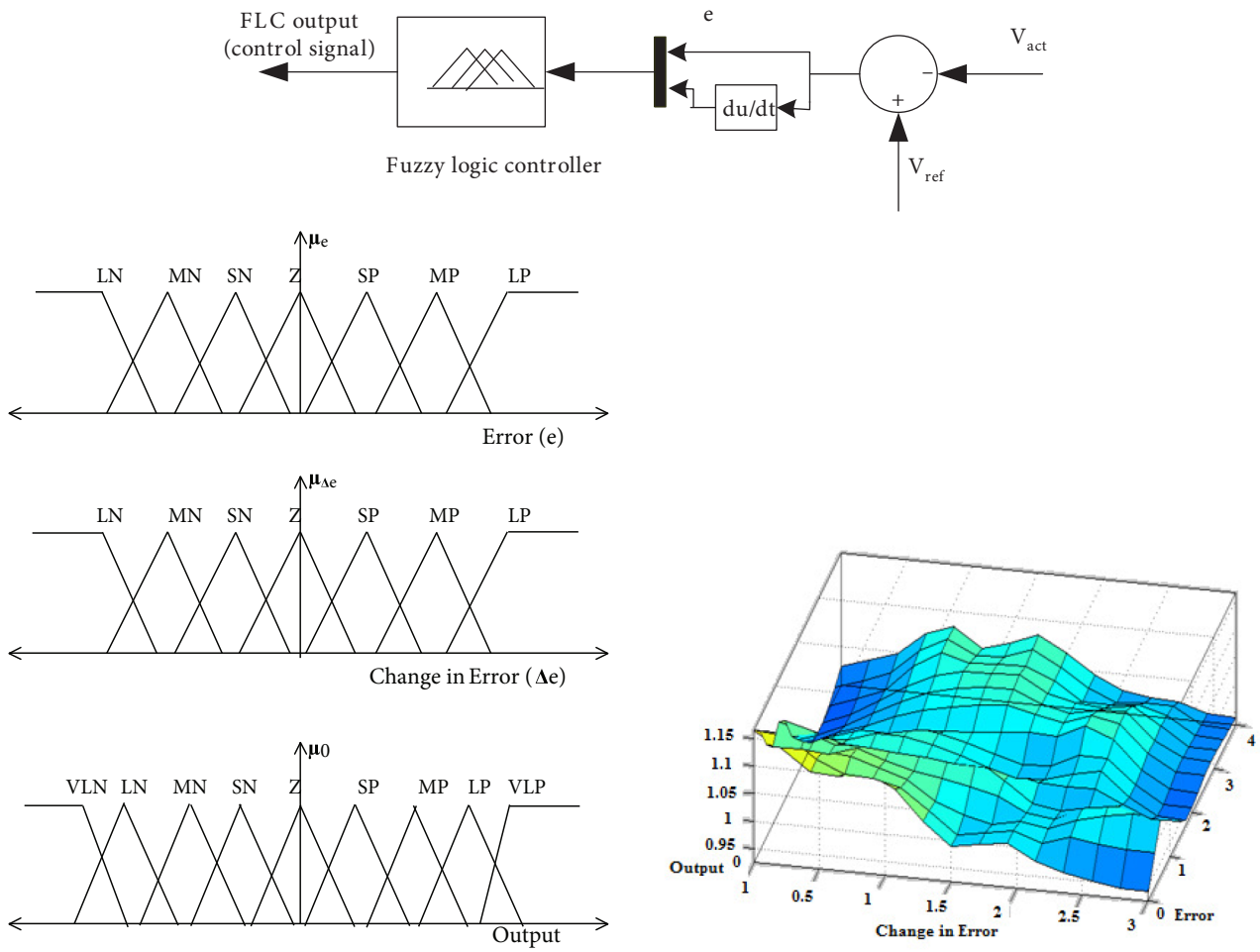

Figure 7. (a) Schematic diagram of the FLC controller, (b) Input and output membership functions. (c) Surface plot for the output with various FLC inputs.

The second stage is the fuzzy rule base, which defines relations between the input fuzzy sets and the output fuzzy sets. The rule base is one that associates the output of the fuzzy controller to its inputs. The rule base is derived by understanding the behavior of the system. The rules are formed using the if-then condition. In the rule base for input fuzzy sets 'F' and 'G' and the output fuzzy sets 'I' the rules are in the form of *If F and G Then I*. The rules can be developed using the knowledge acquired by the designer. The rules for the FLC to control the inverter output voltage are designed here to incorporate the following considerations keeping in view the overall control performance. The control signal at the output of the FLC is based on the following simple linguistic rules.

1) When the change in actual voltage (V_{act}) is more than the reference voltage (V_{ref}) then the change in pulse width must be larger, to bring the output to the reference voltage V_{ref}.

2) A small change in pulse width is enough if the error between V_{act} and V_{ref} is nearer to zero.

3) With the zero error, i.e when V_{act} is equal to V_{ref}, then the change in error is high. To reduce the change in error the pulse width need to be maintained constant.

4) When the actual voltage reaches the reference voltage with small perturbations, the change in pulse width should be small to prevent the output moving from its reference value.

About 49 (7 * 7) rules are developed for the specified control problem based on the listed assumptions. The corresponding fuzzy rule base is given in Table 2. There are several possible combinations of the degree of supports with varying strengths to the corresponding rules, to satisfy the different conditions. The next stage in the FLC is the inference engine. It computes the control output variable based on the individual contributions of each rule discussed in the rule base. The surface plot of the designed FLC is shown in Figure 7(c).

Table 2. Fuzzy rule base.

e/Δe	SN	MN	LN	Z	SP	MP	LP
SN	VLP	SP	LP	SN	Z	VLN	LN
MN	SP	MP	MP	MN	VLN	Z	VLP
LN	MP	VLP	MP	LP	MN	LN	VLN
Z	SP	MP	LP	Z	SN	MN	LN
SP	Z	LN	VLN	Z	SP	MP	MN
MP	SN	Z	VLP	MP	MN	LN	VLN
LP	VLN	MP	Z	MP	VLN	MN	LN

The final stage in the FLC performs the defuzzification. In this, the fuzzified FLC output signal is converted into a precise quantity. In the defuzzification process, the crisp value of the control signal to pulse width is obtained. Defuzzification is performed using the centroid defuzzification technique [24]. The crisp value of the controller output y is computed by

$$y = \frac{\sum \mu_i y_i}{\sum \mu_i}, \tag{38}$$

where mu_i is the ith membership grade of the output y.

Using the above mentioned steps, the fuzzy controller is developed for the control of inverter output voltage. At each sampling time, the actual voltage is sensed using the voltage sensing circuit. The sensed actual voltage is compared with the reference voltage (V_{ref}) to find the error (e), which is equal to $V_{ref} - V_{act}$. By using the error and change in error (Δe) signals, the fuzzy controller determines the control action required from the fuzzy knowledge base. Then it computes the change in the control voltage required for the PWM generation. The PWM generation circuit consists of a logical circuit that compares the carrier signal with the FLC output signal. Whenever the magnitude of the carrier signal is higher than the FLC output signal the PWM generator output is logically high; otherwise it is low as shown in Figure 8.

5.3. Results and discussion

Simulation has been performed to analyze the performance of the two controllers in the system using the MATLAB simulation tool. The following subsections describe the simulation and hardware results.

5.4. Performance of the PID and FLC under no load condition

Based on the above descriptions, the PID controller and FLC are developed and the performance of the converter is evaluated under the no load condition. The gain values of the PID controller tuned under this condition are shown in Table 3. Figures 9(a) and 9(b) show the output voltage (V_o) and output current (I_o) of the inverter, respectively. For the time period up to 0.3 s the V_0 is shown in Figure 9(c) during the unloaded condition.

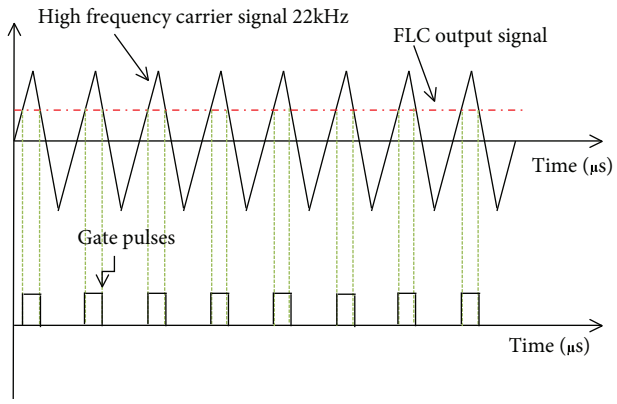

Figure 8. Gate pulse generation using FLC signal.

The time domain specifications of the response of the converter under consideration are rise time, settling time, maximum peak overshoot, and steady state errors. They are obtained from the response of the system under no load condition and they are given in Table 4. The output voltage response of the inverter has large overshoots with the maximum peak overshoot of 30% during the transient time. The response takes 70 ms to get settled to a steady state value. The output voltage (V_o) of the system with the PID and FLC under no load condition is shown in Figures 9(d) and 9(e), respectively. With the conventional PID controller, the peak overshoot and the settling time are reduced to 11% and 40 ms. With the FLC, overshoots are completely eliminated and the response gets settled with the settling time of 0.5 ms. Figure 9(f) shows the RMS value of the V_o with the PID controller and the FLC. It can be seen from the waveforms that the FLC based system has improved dynamic response compared to the PID controlled system.

Table 3. Gains of the PID controller under no load condition.

Parameter	Symbol	Value
Proportional gain	K_p	0.5
Integral gain	K_i	2
Differential gain	K_d	0.05

Table 4. Comparison of time domain specifications in open loop and closed loop systems at no load conditions.

Specifications	Open loop response	PID controller	Fuzzy logic controller
Rise time (t_r)	0.7 ms	0.5 ms	0.4 ms
Setting time (t_s)	70 ms	40 ms	0.5 ms
Peak overshoot (% M_p)	30 %	11 %	0.3 %
Steady state error (e_{ss})	3 V	1.5 V	0.03 V

5.5. Performance of the PID controller and FLC under loading condition

Whenever the workpiece is placed inside the work coil the output voltage decreases due to the change in the value of the parameters. In the simulation study, the change in R_{eq} and L_{eq} is incorporated by including the series R_W L_W branch into the circuit at 0.5 s. For the R_{eq} of 5 Ω, 6 Ω, and 6.5 Ω and L_{eq} of 0.06 mH, 0.07 mH, and 0.08 mH the system responses are studied. Figure 10(a) shows the output voltage waveform corresponding to $R_{eq} = 5$ Ω and $L_{eq} = 0.06$ mH and it is observed that effective voltage across the load gets decreased at 0.5 s. The change in the voltage can be clearly observed with the RMS value of the output voltage

shown in Figure 10(b). The fuzzy based control scheme is included in the system in maintaining the load voltage regulation by sensing the output voltage. Figures 10(c) and 10(d) illustrate the instantaneous output voltage with the PID controller and FLC, respectively. Figure 10(e) shows the comparison of the controller response under loading condition. It can be seen from the response that FLC works well for smooth transition of load voltage from reduced value to its normal value, whereas the PID controller creates an oscillation during the transition. The control action of the FLC system is faster than that of the PID controller system. The response of the PID controller is better with fixed gain for that particular load change. To test the adaptive nature of the FLC system the load parameters are varied. For the variation in the load parameters the voltage regulation is achieved with good accuracy using the FLC by maintaining the RMS value of the voltage at 32 V. The output voltages with different values of load parameters are given in Table 5.

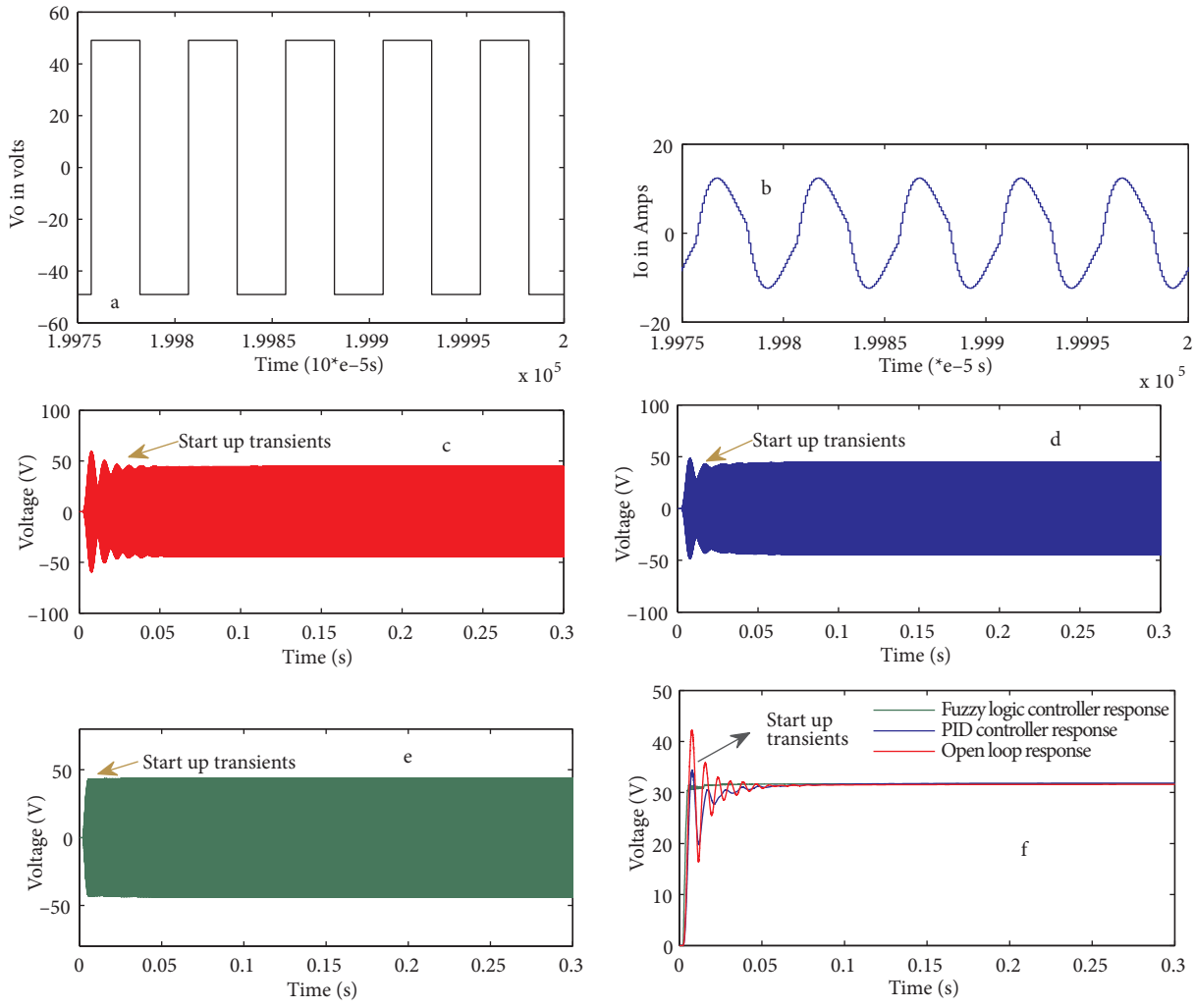

Figure 9. Response under no load condition (a) Output voltage, (b) Output current, (c) Output voltage (V_o) without controller up to 0.3 s, (d) Output voltage with PID controller, (e) Output voltage with FLC, (f) RMS output voltage with FLC and PID controller.

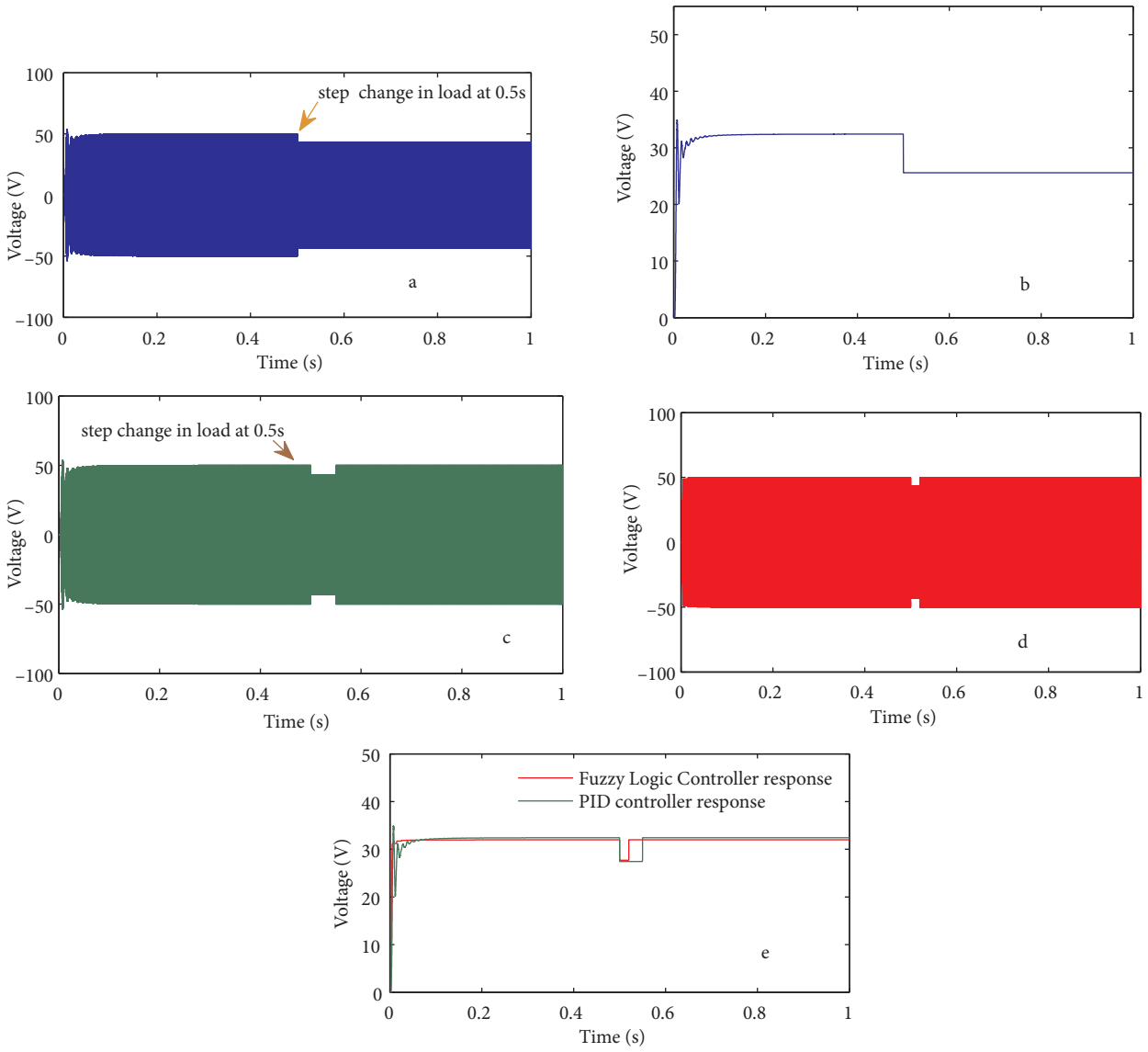

Figure 10. (a) Response under the loading action at 0.5 s, (b) RMS value of the output voltage, (c) Output voltage with PID controller, (d) Output voltage with FLC, (e) RMS voltage waveforms with fuzzy and PID controller.

Table 5. Output voltage for different values of load parameters.

$R_w(\Omega)$	L_w (mH)	V_{ref}(V)	V_0(V)	RMS output voltage (V)
5.5	0.06	48	47.6	32.08
6	0.07	48	47.2	32.06
6.5	0.08	48	47.1	32.05

The instantaneous output voltage and the RMS value of voltage with FLC for the second set of load parameters are given in Figures 11(a) and 11(b), respectively. The instantaneous output voltage and the RMS output voltage with the FLC for the third set of load parameters are given in Figures 11(c) and 11(d), respectively.

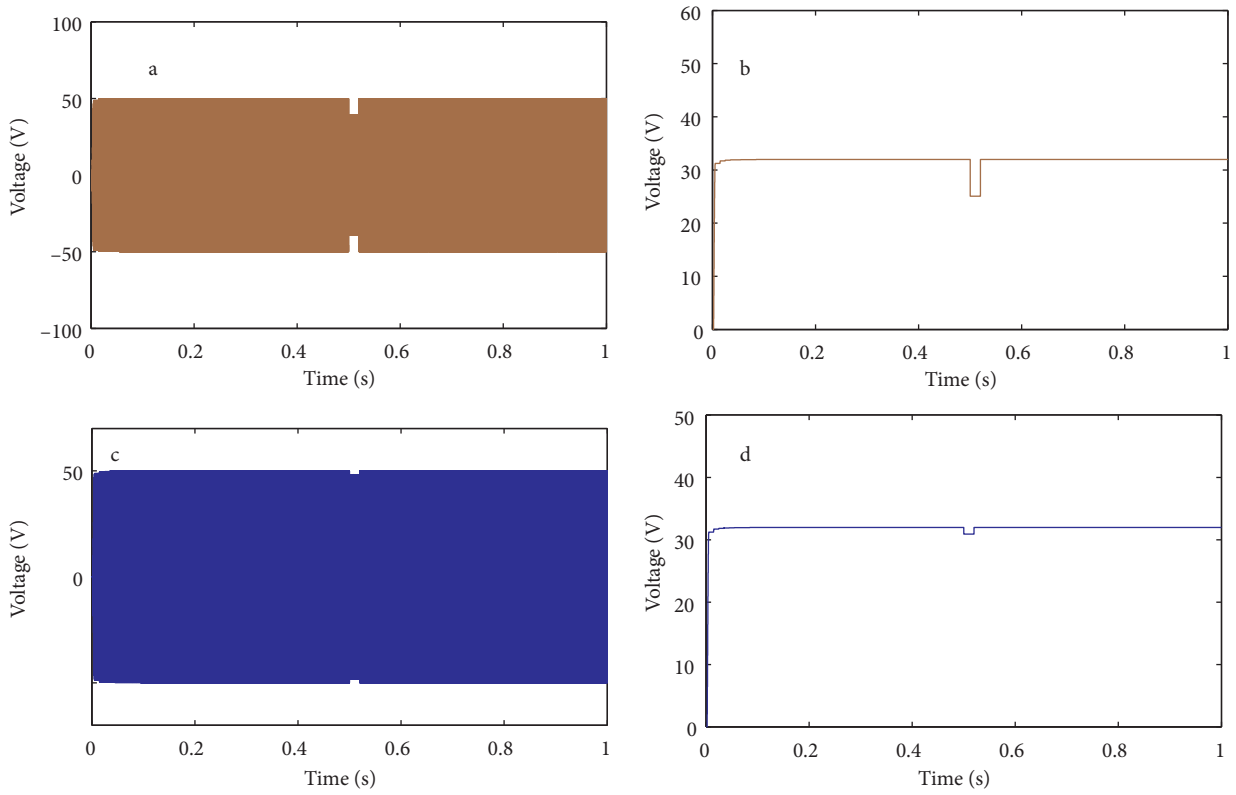

Figure 11. (a) The output voltage waveform with FLC under the loading action at 0.5 s for second set of load parameters, (b) RMS value of the output voltage with FLC, (c) Output voltage with FLC for third set of load parameters, (d) RMS voltage waveforms with FLC.

The time domain specifications of the response of the closed loop system with the FLC and PID controller under different load conditions are given in Table 6. The PID controller controls the inverter output voltage only for the one set of load parameters since it is tuned for the corresponding system gain. It can be seen from the results that the FLC controls the voltage for all variation in equivalent load parameters. From the studies, it can be observed that the system with the FLC has less settling time and steady state error compared to the PID controller based system. The results show that the load adaptive FLC scheme improves the dynamic response of the IH power supply system during start-up and initial loading conditions. The steady state error is also reduced compared to the PID controller.

Table 6. Comparison of time domain specifications under different load conditions.

Specifications	PID controller ($K_p = 13$, $K_i = 0.77$, $K_d = 0.004$)			Fuzzy logic controller		
R_w (Ω)	5.5	6	6.5	5.5	6	6.5
L_w(mH)	0.06	0.07	0.08	0.06	0.07	0.08
Settling time (ms)	1.02	*	*	0.51	0.53	.52
Steady state error (V)	0.04	*	*	0.01	0.01	0.03

*- High for the given gains of PID controller.

The proposed FLC system provides a fast response. However, it requires complete knowledge of the system to develop the rule base.

The efficiency of the converter for different values of output power is shown in Figure 12. From the graph, it is observed that efficiency of the converter is greater compared to the converter without the PLL due to the reduction in switching losses. The efficiency of the system is high since the inverter is operated closer to the resonant frequency by the frequency trailing loop.

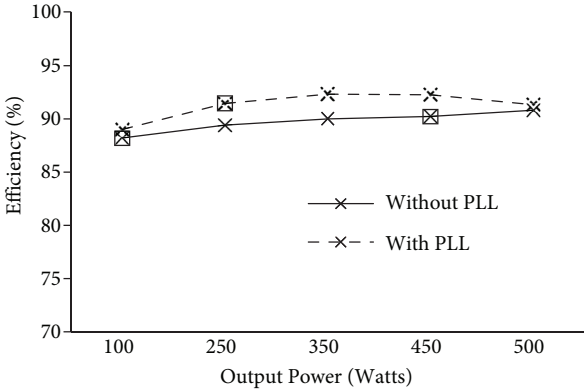

Figure 12. Efficiency vs. output power of the converter.

5.6. Experimental results

The hardware of the single phase HFAC converter is implemented for a prototype model of IH load and it is tested for the required performance. The prototype model of the power supply system for the IH load is shown in Figure 13(a). The power circuit has a diode bridge rectifier, half bridge inverter, and IH load. The rectifier was constructed using IN5408 diode switches. A half bridge inverter was employed for DC-AC conversion. Power switches are IRF840 type MOSFET switches. IH load was built using a copper coil having an outer diameter of 110 mm and thickness of 8 mm. Iron piece of size 100-80-45 mm has been chosen as the workpiece. The coil and the workpiece are selected to match simulation parameters.

The input 50 Hz AC and high frequency AC output voltage waveforms are shown in Figure 13(b). The fuzzy control algorithm is implemented using a PIC16F87A microcontroller. The controller output is driven through an IR2110 driver circuit to the rectifier switches. The driver amplifies the control pulses and it also provides isolation between the control circuit and the power circuit. The high frequency output voltage and current waveforms are shown in Figure 13(c). The load current is measured using the SIGLENT CP4060 type current probe. Expanded views of the output voltage and current are shown in Figures 13(d) and 13(e), respectively. The oscillograms are recorded using the RIGOL DS1052E type digital oscilloscope. The response of the fuzzy logic based system is given in Figure 13(f). The results confirm the effectiveness of the controller in improvement in the dynamic response of the IH system.

5.7. Conclusion

FLC based control of a high frequency converter is proposed to perform the voltage regulation for an IH system. The state space modelling of the IH system is done to study the operating conditions. The dynamic response of the IH system is evaluated with the PID controller and FLC. The performance of the control scheme is studied with both the controllers under no load and various load conditions. Hardware implementation of the IH power supply system is performed to study the controller response. The results show that the system with FLC improves the response with lower rise time, settling time, and steady state error. FLC also performs the voltage regulation for wide load variations compared to the conventional PID controller.

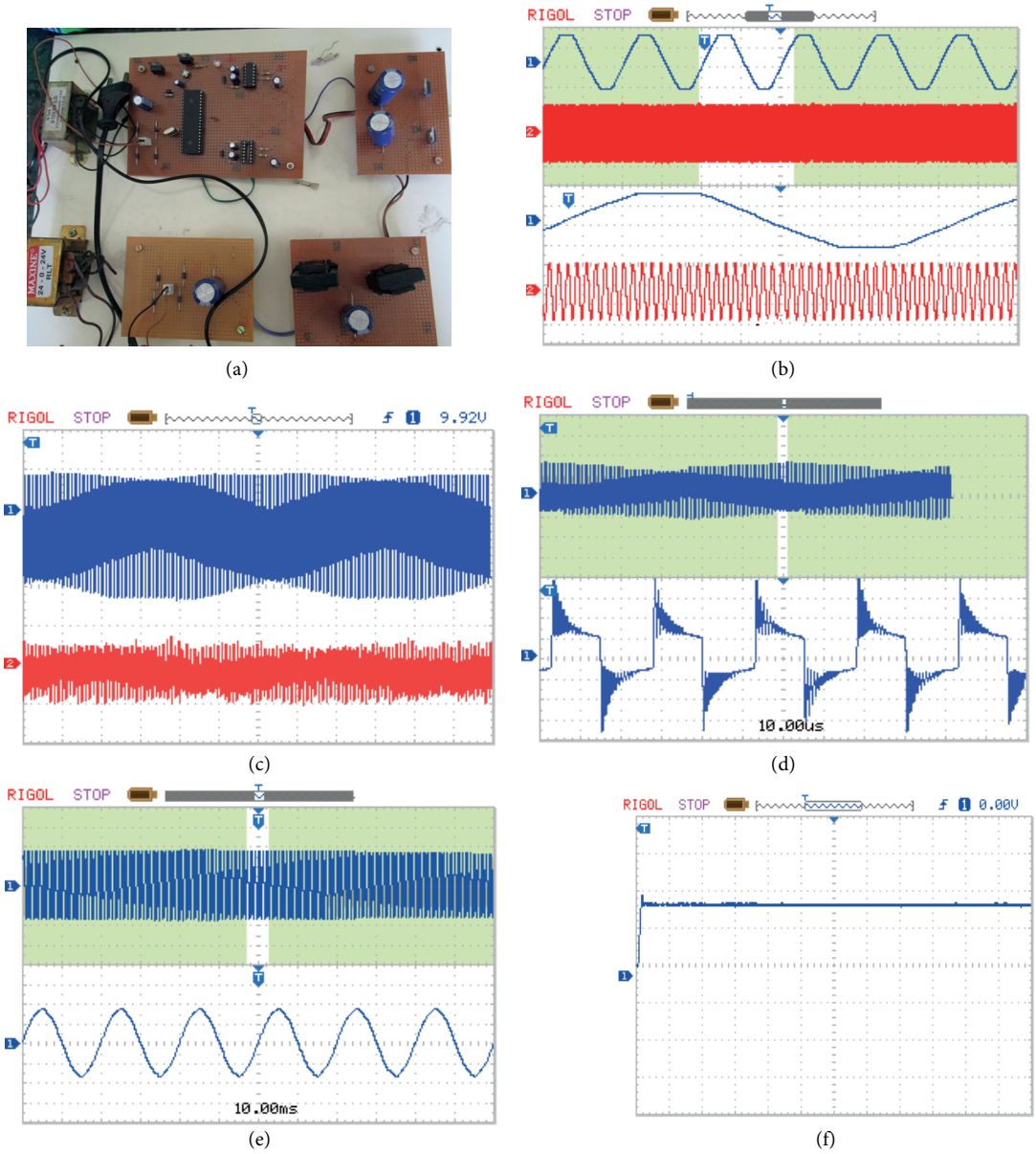

Figure 13. (a) Hardware layout of IH power supply system, (b) Input 50 Hz AC voltage and 22 kHz output voltage ("X Axis 10 ms/div, Y axis 20 V/div"), (c) Output voltage and current of inverter ("X Axis 20 ms/div, Y Axis 1 cm = 20 V/div, 10 A/div"), (d) Expanded view of output voltage ("X Axis 20 *mu* s/div, Y Axis 20 V/div"), (e) Expanded view of Output current ("X Axis 25 *mu* s/div, Y Axis 10 A/div"), (f) Voltage response of the system with FLC for unloaded condition ("X Axis 25 *mu* s/div, Y Axis 15 V/div").

References

[1] Ye Z, Jain PK, Sen PC. A full-bridge resonant inverter with modified phase-shift modulation for high-Frequency AC power distribution systems. IEEE T Ind Electron 2007; 54: 2831-2845.

[2] Li Z, Park CH, Kwon JM, Kwon BH. High-power-factor single-stage LCC resonant inverter for liquid crystal display backlight. IEEE T Ind Electron 2011; 58: 1008-1015.

[3] Lucía O, Barragán LA, Burdío JM, Jiménez O, Navarro D, Urriza I. A versatile power electronics test-bench architecture applied to domestic induction heating. IEEE T Ind Electron 2011; 58: 998-1007.

[4] Saha B, Kwon SK, Ahmed NA, Omori H, Nakaoka M. Commercial frequency AC to high frequency AC converter with boost-active clamp bridge single stage ZVS-PWM inverter. IEEE T Power Electron 2008; 23: 412-419.

[5] Espí Huerta JM, Dede García Santamaría EJ, García Gil R, Castello Moreno J. Design of the L-LC resonant inverter for induction heating based on its equivalent SRI. IEEE T Ind Electron 2007; 54: 3178-3187.

[6] Okudaira S, Matsuse K. Adjustable frequency quasi-resonant inverter circuits having short-circuit switch across resonant capacitor. IEEE T Ind Electron 2008; 23: 1830-1838.

[7] Chudjuarjeen S, Sangwang A, Koompai C. An improved LLC resonant inverter for induction-heating applications with asymmetrical control. IEEE T Ind Electron 2011; 58: 2915-2925.

[8] Ahmed NA, Nakaoka M. Boost-half-bridge edge resonant soft switching PWM high-frequency inverter for consumer induction heating appliances. IEE Proc Electr Power Appl 2006; 153: 932-938.

[9] Kifune H, Hatanaka Y, Nakaoka M. Cost effective phase shifted pulse modulation soft switching high frequency inverter for induction heating applications. IEE Proc Electr Power Appl 2004; 151: 19-25.

[10] Lucia O, Burdio JM, Millan I, Acero J, Puyal D. Load-adaptive control algorithm of half-bridge series resonant inverter for domestic induction heating. IEEE T Ind Electron 2009; 56: 3106-3116.

[11] Lucía O, Burdío JM, Barragán LA, Acero J, Millán I. Series-resonant multi inverter for multiple induction heaters. IEEE T Power Electron 2010; 25: 2860-2868.

[12] Kamli M, Yamamoto S, Abe M. A 50-150 kHz half-bridge inverter for induction heating applications. IEEE T Ind Electron 1996; 43: 163-172.

[13] York B, Yu W, Lai JS. Hybrid-frequency modulation for PWM-integrated resonant converters. IEEE T Power Electron 2013; 28: 985-994.

[14] Sarnago H, Lucía O, Mediano A, Burdío JM. Modulation scheme for improved operation of a RB-IGBT based resonant inverter applied to domestic induction heating. IEEE T Ind Electron 2013; 60: 2066-2073.

[15] Sarnago H, Mediano A, Lucia O. High efficiency AC–AC power electronic converter applied to domestic induction heating. IEEE T Power Electron 2012; 27: 3676-3683.

[16] Lucía O, Acero J, Carretero C, Burdío JM. Induction heating appliances: towards more flexible cooking surfaces. IEEE Industrial Electronics Magazine 2013; 7: 35-47.

[17] Booma N, Rama Reddy S. Design and simulation of energy efficient fixed frequency pulse controlled power converter for induction melting application. Advanced Materials Research 2013; 768: 404-410.

[18] Sarnago H, Lucia O, Mediano A, Burdio JM. Class-D/DE dual-mode-operation resonant converter for improved-efficiency domestic induction heating system. IEEE T Power Electron 2013; 28: 1274-1285.

[19] Meng L, Cheng KWE, Chen KW. Systematic approach to high power and energy-efficient industrial induction cooker system: circuit design, control strategy, and prototype evaluation. IEEE T Power Electron 2011; 26: 3754-3365.

[20] Okuno A, Kawano H, Sun J, Kurokawa M, Kojina A, Nakaoka M. Feasible development of soft-switched SIT inverter with load-adaptive frequency-tracking control scheme for induction heating. IEEE T Ind Appl 1998; 34: 713-718.

[21] Okuno P, Hayashi M, Kawano H, Yasutsune H, Hiraki E, Nakaoka M. Phase-lock loop operated load-resonance inverter using static induction power transistors and its practical characteristic evaluations. International IEEE/IAS Conference on Industrial Automation and Control: Emerging Technologies. Piscataway, NJ. IEEE, 1995: 1-7.

[22] Ziegler J, Nichols N. Optimum settings for automatic controllers. Trans ASME 1942: 759-768.

[23] Ang K H, Chong G, Li Y. PID control system analysis, design, and technology. IEEE T Contr Sys Tech 2005; 13: 559-576.

[24] Chitra A, Meenakshi T, Asha J. Fuzzy logic controller for cascaded H-bridge multilevel inverter. International Journal of Engineering Science and Technology 2011; 3: 1378-1386.